# Electric fields and zonal winds in the equatorial ionosphere inferred from CHAMP satellite magnetic measurements

Stefan Maus,[1,2] Patrick Alken,[1,2] and Hermann Lühr[3]

Received 5 June 2007; revised 5 October 2007; accepted 22 October 2007; published 1 December 2007.

[1] The Equatorial Electrojet (EEJ) produces a strong magnetic signal in measurements of the low-orbiting CHAMP satellite. Six years of data with more than 30,000 dayside equator crossings provide a unique data basis to study this current system. In addition to scalar measurements used in previous studies, we have also inverted vector magnetic field measurements to gain accurate meridional profiles of the eastward current in the equatorial region. By solving the relevant differential equation, the CHAMP-derived current profiles can be inverted for the driving zonal electric fields and zonal winds. As a result of this feasibility study, we suggest an inversion of the complete set of individual CHAMP EEJ current profiles, which will provide valuable new information on dayside electric fields and thermospheric winds at low latitudes. **Citation:** Maus, S., P. Alken, and H. Lühr (2007), Electric fields and zonal winds in the equatorial ionosphere inferred from CHAMP satellite magnetic measurements, *Geophys. Res. Lett.*, *34*, L23102, doi:10.1029/2007GL030859.

## 1. Introduction

[2] The equatorial electrojet (EEJ) is an intense eastward electric current following the magnetic dip equator in the lower ionosphere [*Forbes*, 1981; *Onwumechili*, 1997]. Satellite studies of the EEJ have been reported for POGO by *Cain and Sweeney* [1973], for Magsat by *Langel et al.* [1993] and Ørsted by *Jadhav et al.* [2002] and *Ivers et al.* [2003]. Exciting new measurements for EEJ studies have become available since July 2000 with the launch of the CHAMP satellite which is measuring the magnetic field in a low-altitude, polar orbit, covering all local times every 130 days. CHAMP magnetic data can be inverted to derive meridional profiles of the height-integrated, eastward current density in the equatorial region [*Lühr et al.*, 2004]. This inversion takes into account the satellite altitude and various geometrical effects that affect the magnetic signal produced by the EEJ. These CHAMP current profiles showed for the first time that the EEJ peaks exactly at the magnetic dip equator at all local times and longitudes. Following up on studies by *Anderson et al.* [2002], *Alken and Maus* [2007] found a high correlation between the eastward electric field inferred from CHAMP current observations and vertical drifts measured by the JULIA radar [*Hysell et al.*, 1997], further establishing the EEJ as a useful proxy for the dayside eastward electric field. *Alken and Maus* [2007] also produced a climatological model for the peak strength and day-to-day variability of the EEJ as a function of local time, longitude, season and solar activity (http://geomag.org/models/EEJ.html).

[3] Inversions of CHAMP magnetic data have added a new dimension to EEJ studies by providing a complete meridional profile of the zonal current in a 20° band along the dip equator, rather than just a single EEJ current estimate. Except during sunrise, when the EEJ is usually reversed, the profiles typically show an eastward current at the dip equator, flanked by westward "return" currents, peaking at ±5° north and south of the dip equator. The overall shape of these meridional current profiles is well determined by the satellite observations. However, there is an inherent uncertainty in the zero-level of the eastward current. This uncertainty comes in two flavors: The first is due to the technical difficulty of separating the EEJ magnetic signal from the background magnetic field caused by the Sq current system and the magnetospheric ring current. As pointed out by *Lühr and Maus* [2006], this first uncertainty can be overcome by using the magnetic field vector components in addition to the field intensity. A second uncertainty arises from the fact that a wide eastward current sheet with little meridional variability produces a magnetic field signal that is hardly discernible from the background magnetic field. Therefore, our satellite derived meridional current profiles have to be considered as additional currents, relative to an unknown zero-current level. Indeed, as shown by *Fambitakoye et al.* [1976] and reviewed by *Forbes* [1981, p. 492], the combined effect of an eastward electric field and a westward wind produces a current profile similar in shape to the ones derived from CHAMP, but shifted upward, so that even in the side lobes the total current is oriented eastward.

[4] Building on earlier investigations [*Sugiura and Poros*, 1969; *Richmond*, 1973], we invert satellite-derived meridional profiles of the eastward current for E-layer zonal electric fields and for zonal winds. The procedure is demonstrated on mean current profiles in four different local time sectors. The results indicate that an inversion of the complete set of individual current profiles, while computationally more expensive, would yield valuable information on zonal electric field and wind variations.

## 2. Observations

[5] The CHAMP satellite was launched in July 2000 into a near-polar orbit at 460 km altitude [*Reigber et al.*, 2002].

[1]Cooperative Institute for Research in Environmental Science, University of Colorado, Boulder, Colorado, USA.
[2]NOAA National Geophysical Data Center, Boulder, Colorado, USA.
[3]GeoForschungsZentrum Potsdam, Potsdam, Germany.


0094-8276/07/2007GL030859$05.00

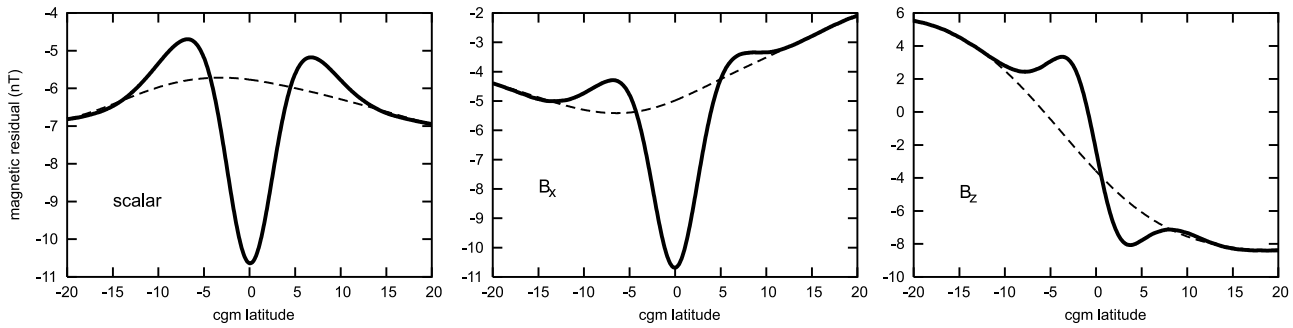


**Figure 1.** Average CHAMP magnetic residuals (solid line) on meridional profiles across the magnetic dip equator. The background field (dashed) is fitted outside of a ±12° latitude window. The difference between the residual and the background is inverted in terms of height-integrated eastward current profiles. (left) The scalar inversions were performed on data, while the vector inversions simultaneously fitted the (middle) $B_x$ and (right) $B_z$ residuals.

Over the past 6 years, the orbital altitude has gradually decreased to about 350 km. The mission is expected to last into 2009. With 87.3° inclination, CHAMP passes the equator almost exactly in the meridional direction. CHAMP drifts in local time, covering all local time sectors in about 130 days. The relevant instruments for this study are the scalar magnetometer, measuring the field intensity, and the vector magnetometer whose orientation in space is determined by a dual-head star camera.

[6] The eastward EEJ is visible on the dayside as a prominent depression in CHAMP scalar magnetic measurements. In a previous study [*Lühr et al.*, 2004], we inverted the scalar measurements for parallel line currents at E-layer altitude (108 km); each line current representing a 0.5 degree wide band of height-integrated eastward current. We found that the eastward EEJ is flanked by westward return currents. However, difficulties in separating the background magnetic field from the EEJ signal translated into uncertainties in the zero-level for the current profile. This is illustrated in Figure 1. Choosing a lower background magnetic field (dashed line) would strengthen the side lobes, thus resulting in higher estimates of the flanking return currents. In a recent study of vector magnetic field residuals, *Lühr and Maus* [2006] confirmed the existence of the negative side-lobes.

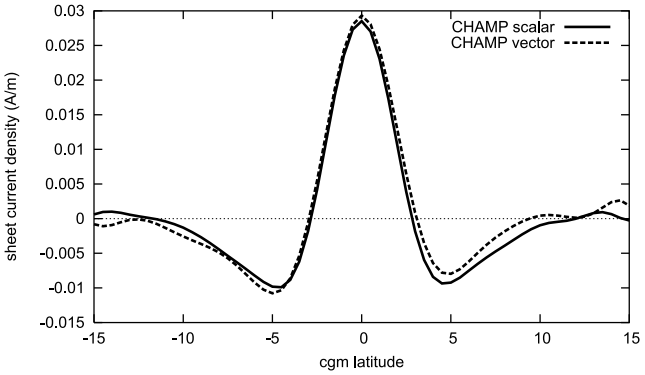


**Figure 2.** Average CHAMP meridional profiles of the eastward current. Independent inversions of the scalar and vector magnetic residuals lead to almost identically shaped current profiles.

[7] For the present study, independent inversions of scalar and vector data were carried out in order to validate a common zero-level. We further improved the inversion technique, replacing the infinite line-current assumption with a numerical 3D simulation of line current segments in corrected geomagnetic (cgm) coordinates [*Richmond*, 1995]. The independent inversion results from the scalar and vector data sets (Figure 2) are in good agreement when the background magnetic field is removed by fitting the data outside of a window of ±12° in latitude. We also verified that the current profiles obtained from two higher satellites, Ørsted and SAC-C, are in good agreement with CHAMP when using the same window and inversion scheme. In the earlier study [*Lühr et al.*, 2004] we used a wider window of ±15°, leading to a slightly higher zero-level, corresponding to stronger return currents.

## 3. Modeling

[8] The CHAMP-derived meridional current profiles can be explained by two sources: The E-region dynamo zonal electric field [*Heelis*, 2004] and zonal winds which are likely responsible for the "return" currents [*Forbes*, 1981, p. 492]. The governing equations in spherical coordinates (radius $r$, co-latitude $\vartheta$, longitude $\vartheta$) are

$$\nabla \times \mathbf{E} = 0 \tag{1}$$

$$\mathbf{J} = \nabla \times \psi \hat{\boldsymbol{\varphi}} + J_\varphi \hat{\boldsymbol{\varphi}} = \underline{\sigma}\left(\mathbf{E} + u_\varphi \hat{\boldsymbol{\varphi}} \times \mathbf{B}\right), \tag{2}$$

where $\mathbf{J}$ is the current density, $\psi$ is the stream function of the meridional current system, $\hat{\boldsymbol{\varphi}}$ is a unit vector in the eastward direction, $\underline{\sigma}$ is the conductivity tensor [*Forbes*, 1981, equation 10], $\mathbf{E}$ is the electric field, $u_\varphi$ is the eastward wind, and $\mathbf{B}$ is the ambient magnetic field given by a main field model. Assuming that all quantities are constant in the eastward direction leads to six component equations

$$\left.\begin{aligned}\partial_\vartheta\left(\sin\vartheta E_\varphi\right) &= 0\\ \partial_r\left(rE_\varphi\right) &= 0\end{aligned}\right\} \Rightarrow E_\varphi = \frac{RE_0}{r\sin\vartheta} \tag{3}$$

$$\partial_r(rE_\vartheta) - \partial_\vartheta E_r = 0 \tag{4}$$

$$\frac{\partial_\vartheta}{r\sin\vartheta}(\sin\vartheta\psi) = \sigma_{rr}E_r + \sigma_{r\vartheta}E_\vartheta + \sigma_{r\varphi}E_\varphi - \sigma_P B_\vartheta u_\varphi \quad (5)$$

$$-\frac{\partial_r}{r}(r\psi) = \sigma_{\vartheta r}E_r + \sigma_{\vartheta\vartheta}E_\vartheta + \sigma_{\vartheta\varphi}E_\varphi + \sigma_P B_r u_\varphi \quad (6)$$

$$J_\varphi = \sigma_{\varphi r}E_r + \sigma_{\varphi\vartheta}E_\vartheta + \sigma_{\varphi\varphi}E_\varphi + \sigma_H|B|u_\varphi \quad (7)$$

where $E_0$ is the equatorial eastward electric field at the reference radius $R$, and $\sigma_p$ and $\sigma_H$ are the Pederson and Hall conductivities, respectively. Combining (4), (5) and (6) and eliminating $E_r$ and $E_\vartheta$ gives a second-order, elliptical partial differential equation (PDE) for the stream function $\psi$ as

$$\begin{aligned}
&\left[\left(\frac{1}{r}+\partial_r\right)\left(\frac{\cos\vartheta}{r\alpha\sin\vartheta}+\frac{\sigma_{rr}}{r\alpha\sigma_{\vartheta r}}\right)-\frac{\partial_\vartheta}{r^2}\left(\frac{\cos\vartheta}{\gamma\sin\vartheta}+\frac{\sigma_{r\vartheta}}{\gamma\sigma_{\vartheta\vartheta}}\right)\right]\psi\\
&+\left[\frac{2\sigma_{rr}}{r\alpha\sigma_{\vartheta r}}+\frac{\cos\vartheta}{r\alpha\sin\vartheta}+\partial_r\left(\frac{\sigma_{rr}}{\alpha\sigma_{\vartheta r}}\right)-\frac{\partial_\vartheta}{r}\left(\frac{\sigma_{r\vartheta}}{\gamma\sigma_{\vartheta\vartheta}}\right)\right]\partial_r\psi\\
&+\left[\frac{\partial_r}{r}\left(\frac{1}{\alpha}\right)-\frac{\cos\vartheta}{r^2\gamma\sin\vartheta}-\frac{\sigma_{r\vartheta}}{r^2\gamma\sigma_{\vartheta\vartheta}}-\frac{\partial_\vartheta}{r^2}\left(\frac{1}{\gamma}\right)\right]\partial_\vartheta\psi\\
&+\frac{\sigma_{rr}}{\alpha\sigma_{\vartheta r}}\partial_r^2\psi-\frac{1}{r^2\gamma}\partial_\vartheta^2\psi+\left(\frac{1}{r\alpha}-\frac{\sigma_{r\vartheta}}{r\gamma\sigma_{\vartheta\vartheta}}\right)\partial_\vartheta\partial_r\psi\\
&=\left(\frac{1}{r}+\partial_r\right)\left(\frac{\beta}{\alpha}\right)-\frac{\partial_\vartheta}{r}\left(\frac{\delta}{\gamma}\right) \quad (8)
\end{aligned}$$

where

$$\alpha = \sigma_{r\vartheta} - \frac{\sigma_{rr}}{\sigma_{\vartheta r}}\sigma_{\vartheta\vartheta} \quad (9)$$

$$\beta = \left(\sigma_{r\varphi} - \frac{\sigma_{rr}}{\sigma_{\vartheta r}}\sigma_{\vartheta\varphi}\right)E_\varphi - \left(B_\vartheta + \frac{\sigma_{rr}}{\sigma_{\vartheta r}}B_r\right)\sigma_P u_\varphi \quad (10)$$

$$\gamma = \sigma_{rr} - \frac{\sigma_{r\vartheta}}{\sigma_{\vartheta\vartheta}}\sigma_{\vartheta r} \quad (11)$$

$$\delta = \left(\sigma_{r\varphi} - \frac{\sigma_{r\vartheta}}{\sigma_{\vartheta\vartheta}}\sigma_{\vartheta\varphi}\right)E_\varphi - \left(B_\vartheta + \frac{\sigma_{r\vartheta}}{\sigma_{\vartheta\vartheta}}B_r\right)\sigma_P u_\varphi \quad (12)$$

We solve this PDE in the latitude range of $-25°$ to $25°$ and the altitude range of 65 km to 465 km on a $0.5° \times 2$ km mesh, using a standard finite difference approach with a 9-cell stencil. As boundary conditions we demand that the stream function vanishes at the upper and lower boundaries, and its normal derivative vanishes at the northern and southern boundaries. The resulting finite difference system of linear equations is solved using a sparse matrix algorithm. Once the stream function $\psi$ has been determined, the electric fields $E_r$ and $E_\vartheta$ follow from equations (4) to (6) and the eastward current density is given by (7).

[9] To set up the conductivity tensor $\underline{\sigma}$, one has to know the densities and temperatures of the electrons, ions and neutrals. We take this information from the International Reference Ionosphere [*Bilitza*, 2001] and the thermospheric model NRLMSISE-00 [*Picone et al.*, 2002]. The ambient geomagnetic field is taken from the POMME-3 main field model [*Maus et al.*, 2006].

[10] A key issue in the proposed inversion method is that the meridional current profile is a linear function of the eastward electric field and the zonal wind. This offers the opportunity to compute the individual responses to a unit eastward electric field and to each member of a set of B-spline basis functions for the wind. The CHAMP-derived E-region current profile can then be inverted for the eastward electric field and a vertical profile of the zonal wind in a linear least-squares inversion. We use one parameter for the equatorial eastward electric field $E_0$, a parameter $J_0$ for the zero-current level, and six wind parameters for cubic B-splines with knots at 90, 100, 110, 120, 130, 140, 160, 190, and 240 km. The wind correction given by these splines is forced to zero below 90 km and remains constant above 240 km altitude.

[11] Due to an ambiguity between the effect of an eastward electric field and an E-region zonal wind, it is difficult to simultaneously invert for both. We therefore propose to either fix the wind and invert for the electric field or to fix the field and invert for the wind. The latter inverse problem is well-posed because magnetic field lines are equipotentials of the electric field, and zonal wind effects at different altitudes are mapped to different latitudes in the E-region, influencing different sections of the meridional current profile. There is, however, an ambiguity in the zero-wind level. We therefore invert for the minimum deviation of the zonal wind velocity from the Horizontal Wind Model HWM93 [*Hedin et al.*, 1996]. The penalty function used in the inversion is

$$P(\mathbf{m}) = C_J \sum_{i_\vartheta=0}^{49}\left[J_\varphi^{\mathrm{CHAMP}} - J(\mathbf{m})\right]^2 + C_u \sum_{i_r=0}^{200}\left[u_\varphi^{\mathrm{HWM}} - u_\varphi(\mathbf{m})\right]^2 \quad (13)$$

where $\mathbf{m}$ is the vector of model coefficients, $C_J = 1\ m^2/A^2$, and $C_u = 10^{-9}\ s^2/m^2$ is the damping coefficient for the wind.

## 4. Results

[12] The modeling scheme proposed here can be applied to individual satellite passes across the magnetic equator. For the present proof of concept, however, we only interpreted average profiles for four representative local time sectors. The averages in every local time sector were taken over all passes, regardless of magnetic and solar activity, season and longitude. The IRI and NRLMSISE-00 models were evaluated for Kp = 2 and F10.7 = 120, the mean values for the study period, and the resulting conductivities were averaged over all seasons and longitudes. We averaged the magnetic field geometry over all longitudes and ignored the eastward component.

[13] The current profiles inferred independently from CHAMP scalar and vector data were found to be very similar. Since the scalar data have better coverage, and scalar data, in contrast to vector data, are unaffected by attitude noise, we interpreted only the scalar data here. Figure 3 shows the observed and modeled current profiles for four local time sectors, 06-07, 10-11, 14-15 and 17-18 LT. The CHAMP-derived current profiles are shown in black. The blue curve

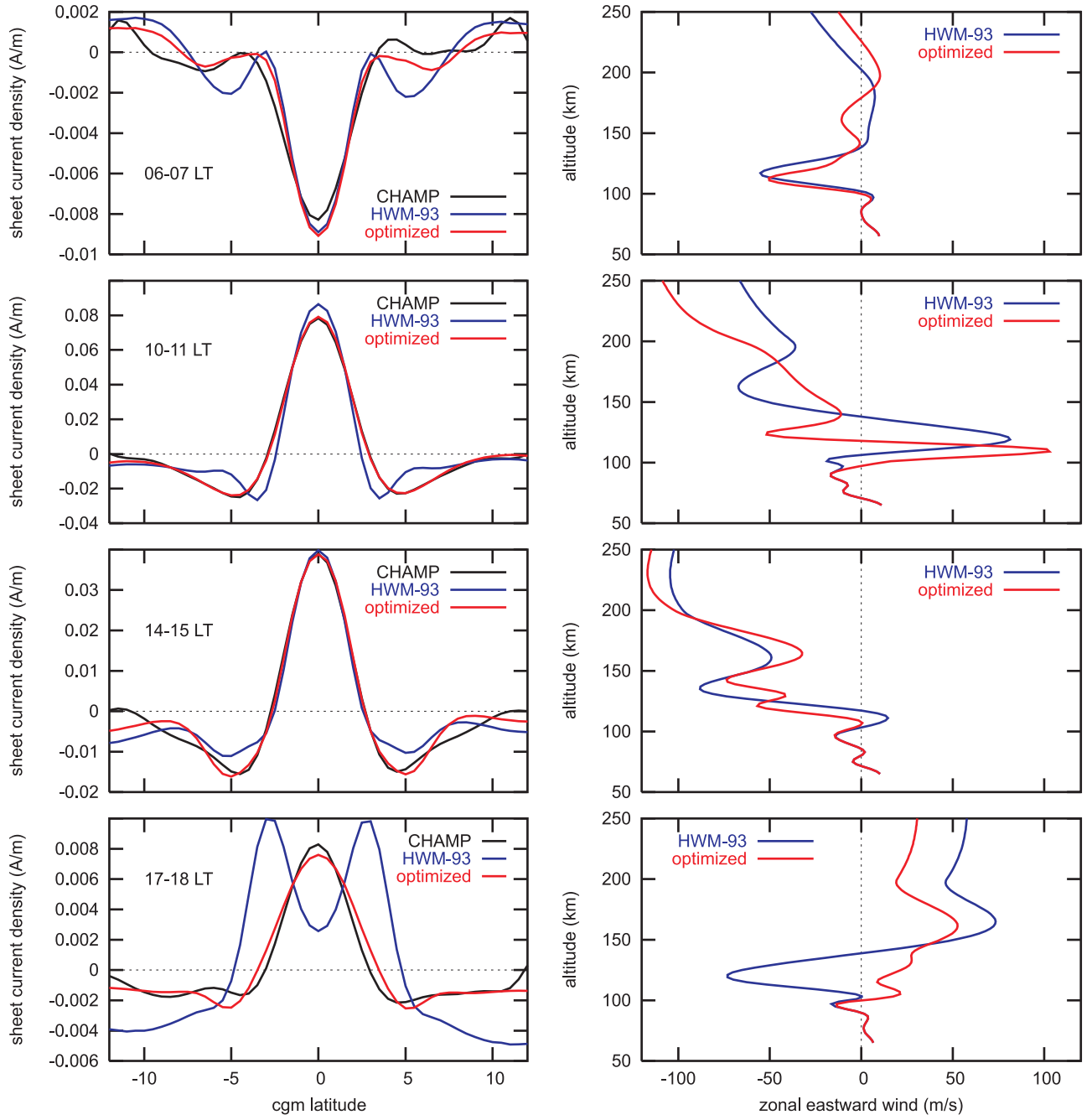


**Figure 3.** (left) Interpretations of average CHAMP-derived current profiles for four different local time sectors; observations in black, the solution for HWM93 zonal winds in blue, and the solution for optimized winds are shown in red. (right) The corresponding vertical wind profiles.

**Table 1.** Inversion Results for the Eastward Electric Field and the Constant Eastward Current Offset for the Four Local Time Sectors Shown in Figure 3[a]

| | HWM93 | | Optimized Wind | |
|---|---|---|---|---|
| LT | $E_\varphi$ mV/m | $J_0$ A/m | Julia $E_\varphi$ mV/m | $J_0$ A/m |
| 06–07 | −0.13 | −0.006 | −0.13[b] | −0.007 |
| 10–11 | 0.38 | 0.078 | 0.40 | 0.089 |
| 14–15 | 0.29 | 0.062 | 0.26 | 0.051 |
| 17–18 | −0.11 | −0.014 | 0.05 | −0.001 |

[a]For the second inversion (right double column) the Julia-observed $E_\varphi$ was imposed.
[b]Assumed value, no Julia observations.

shows the modeled current if the wind is taken "as is" from HWM93. The inversion in that case only optimizes for the strength of the eastward electric field and for a relative shift in current level between the observation and the model. For the red model curves, we imposed the average electric field inferred from Julia 150 km radar echoes [*Hysell et al.*, 1997] and inverted for deviations in the wind velocity, simultaneously minimizing the root-mean-square difference to HWM93, as given by the second term on the right in (13). The HWM93 wind velocity and the optimized velocity are plotted in the adjacent vertical profiles on the right side for each of the four local time sectors. The corresponding

inversion results for the eastward electric field and the constant eastward sheet current offsets are summarized in Table 1. To derive the total current density, the $J_{const}$ values in columns 3 and 5 have to be added to the blue and red curves, respectively, in the graphs of Figure 3 (left). This strengthens the overall westward current at 06-07 LT, but effectively eliminates the westward current component at 10-11 LT and 14-15 LT. In the 17-18 LT sector, taking HWM93 at face value leads to a significantly over-estimated electrojet current. Our inversion then tries to compensate with a westward electric field, leading to an unrealistic double-peaked current signature. The problem is caused by the strong evening-sector westward wind at 100–150 km altitude in HWM93. This westward wind is indeed poorly constrained by observations in HWM93 (J. Emmert, personal communication, 2007). Instead, our optimized solution indicates an eastward wind at E-region altitudes for this local time. However, results obtained so close to the terminator have to be taken with caution since our underlying simple current model may no longer be valid.

## 5. Discussion

[14] The strength of the equatorial electrojet has been investigated in many studies, using ground and satellite based magnetometers. CHAMP has opened a new dimension by providing accurate meridional current profiles. We first established that independent inversions of scalar and vector magnetic measurements lead to almost identical current profiles. Then we devised a scheme to invert these profiles in terms of zonal electric fields and zonal winds. Numerically solving the relevant differential equation, we computed the expected current for a unit eastward electric field and unit zonal wind basis functions. Since the observed currents must be linear combinations of these individual effects, we gained the electric field and zonal winds in linear inversions. To reduce the ambiguity in the solution, we had to impose the electric field when inverting for the zonal wind, and we sought for the wind profile with the smallest root-mean-square deviation from the model HWM93.

[15] The CHAMP-derived current profiles are well explained by a combination of eastward electric fields and zonal winds. So-called ''return'' currents appear to be just depressions in a generally eastward directed current. In the 10-11 and 14-15 LT sectors, the CHAMP-derived eastward electric field is close to the average value inferred from Julia 150 km radar echoes. We find that the CHAMP current profiles place quite a strong constraint on a thermospheric wind model. Despite some non-uniqueness in the inversion, it appears that HWM93 is partly incompatible with the CHAMP observations during evening hours.

[16] Two effects were ignored here: Vertical winds have an effect similar to an eastward electric field [*Forbes*, 1981]. However their climatology is not well known, and they are generally thought to be weak in comparison to horizontal winds. Furthermore, two-stream instabilities effectively pose an upper limit on the EEJ current density [*Richmond*, 1973]. This ''flattening'' may be visible in the statistical distribution of EEJ strengths which will be available after our planned inversion of the individual CHAMP passes.

[17] **Acknowledgments.** Three anonymous reviewers provided numerous helpful comments. The operational support of the CHAMP mission by the German Aerospace Center (DLR) and the financial support for the data processing by the Federal Ministry of Education and Research (BMBF) are gratefully acknowledged.

## References

Alken, P., and S. Maus (2007), Spatio-temporal characterization of the equatorial electrojet from CHAMP, Ørsted, and SAC-C satellite magnetic measurements, *J. Geophys. Res.*, *112*, A09305, doi:10.1029/2007JA012524.

Anderson, D., A. Anghel, K. Yumoto, M. Ishitsuka, and E. Kudeki (2002), Estimating daytime vertical ExB drift velocities in the equatorial F-region using ground-based magnetometer observations, *Geophys. Res. Lett.*, *29*(12), 1596, doi:10.1029/2001GL014562.

Bilitza, D. (2001), International Reference Ionosphere 2000, *Radio Sci.*, *36*, 261–275.

Cain, J. C., and R. E. Sweeney (1973), The POGO data, *J. Atmos. Terr. Phys.*, *35*, 1231–1247.

Fambitakoye, O., P. N. Mayaud, and A. D. Richmond (1976), Equatorial electrojet and regular daily variation S/R/. III: Comparison of observations with a physical model, *J. Atmos. Terr. Phys.*, *38*, 113–121.

Forbes, J. M. (1981), The equatorial electrojet, *Rev. Geophys.*, *19*, 469–504.

Hedin, A. E., et al. (1996), Empirical wind model for the upper, middle and lower atmosphere, *J. Atmos. Terr. Phys.*, *58*, 1421–1447.

Heelis, R. A. (2004), Electrodynamics in the low and middle latitude ionosphere: A tutorial, *J. Atmos. Sol. Terr. Phys.*, *66*, 825–838, doi:10.1016/j.jastp.2004.01.034.

Hysell, D. L., M. F. Larsen, and R. F. Woodman (1997), JULIA radar studies of electric fields in the equatorial electrojet, *Geophys. Res. Lett.*, *24*, 1687–1690, doi:10.1029/97GL00373.

Ivers, D., R. Stening, J. Turner, and D. Winch (2003), Equatorial electrojet from rsted scalar magnetic field observations, *J. Geophys. Res.*, *108*(A2), 1061, doi:10.1029/2002JA009310.

Jadhav, G., M. Rajaram, and R. Rajaram (2002), A detailed study of equatorial electrojet phenomenon using rsted satellite observations, *J. Geophys. Res.*, *107*(A8), 1175, doi:10.1029/2001JA000183.

Langel, R. A., M. Purucker, and M. Rajaram (1993), The equatorial electrojet and associated currents as seen in Magsat data, *J. Atmos. Terr. Phys.*, *55*, 1233–1269.

Lühr, H., and S. Maus (2006), Direct observation of the F region dynamo currents and the spatial structure of the EEJ by CHAMP, *Geophys. Res. Lett.*, *33*, L24102, doi:10.1029/2006GL028374.

Lühr, H., S. Maus, and M. Rother (2004), Noon-time equatorial electrojet: Its spatial features as determined by the CHAMP satellite, *J. Geophys. Res.*, *109*, A01306, doi:10.1029/2002JA009656.

Maus, S., M. Rother, C. Stolle, W. Mai, S. Choi, H. Lühr, D. Cooke, and C. Roth (2006), Third generation of the Potsdam Magnetic Model of the Earth (POMME), *Geochem. Geophys. Geosyst.*, *7*, Q07008, doi:10.1029/2006GC001269.

Onwumechili, C. A. (1997), *The Equatorial Electrojet*, Gordon and Breach, New York.

Picone, J. M., A. E. Hedin, D. P. Drob, and A. C. Aikin (2002), NRLMSISE-00 empirical model of the atmosphere: Statistical comparisons and scientific issues, *J. Geophys. Res.*, *107*(A12), 1468, doi:10.1029/2002JA009430.

Reigber, C., H. Lühr, and P. Schwintzer (2002), CHAMP mission status, *Adv. Space Res.*, *30*, 129–134.

Richmond, A. D. (1973), Equatorial electrojet: I. Development of a model including winds and instabilities, *J. Atmos. Terr. Phys.*, *35*, 1083–1103.

Richmond, A. D. (1995), Ionospheric electrodynamics using magnetic apex coordinates, *J. Geomagn. Geoelectr.*, *47*, 191–212.

Sugiura, M., and D. J. Poros (1969), An improved Model Equatorial Electrojet with a meridional current system, *J. Geophys. Res.*, *74*, 4025–4034.

P. Alken and S. Maus, National Geophysical Data Center, NOAA E/GC1, 325 Broadway, Boulder, CO 80305-3328, USA. (stefan.maus@noaa.gov)

H. Lühr, GeoForschungsZentrum Potsdam, Telegrafenberg, D-14473 Potsdam, Germany.